

Radial density and heat fluxes description in the velocity space: Nonlinear simulations and quasi-linear calculations

J. Médina, M. Lesur, E. Gravier, T. Réveillé, M. Idouakass, T. Drouot, P. Bertrand, T. Cartier-Michaud, X. Garbet, and P. H. Diamond

Citation: [Physics of Plasmas](#) **25**, 122304 (2018); doi: 10.1063/1.5057420

View online: <https://doi.org/10.1063/1.5057420>

View Table of Contents: <http://aip.scitation.org/toc/php/25/12>

Published by the [American Institute of Physics](#)

Radial density and heat fluxes description in the velocity space: Nonlinear simulations and quasi-linear calculations

J. Médina,¹ M. Lesur,¹ E. Gravier,¹ T. Réveillé,¹ M. Idouakass,¹ T. Drouot,¹ P. Bertrand,¹ T. Cartier-Michaud,² X. Garbet,² and P. H. Diamond³

¹Université de Lorraine, CNRS, IJL, F-54000 Nancy, France

²CEA, IRFM, 13108 Saint-Paul-Lés-Durance Cedex, France

³CMTFO and CASS, University of California, San Diego, California 92093, USA

(Received 14 September 2018; accepted 16 November 2018; published online 13 December 2018)

In the context of temperature gradient-driven, collisionless trapped-ion modes in magnetic confinement fusion, we perform and analyse numerical simulations to explore the turbulent transport of density and heat, with a focus on the velocity dimension (without compromising the details in the real space). We adopt the bounce-averaged gyrokinetic code TERESA, which focuses on trapped particles dynamics and allows one to study low frequency phenomena at a reduced computational cost. We focus on a time in the simulation where the trapped-ion modes have just saturated in amplitude. We present the structure in velocity space of the fluxes. Both density and heat fluxes present a narrow (temperature-normalized energy width $\Delta E/T \approx 0.15$) resonance peak with an amplitude high enough for resonant particles to contribute for 90% of the heat flux. We then compare these results obtained from a nonlinear simulation to the prediction from the quasi-linear theory and we find a qualitative agreement throughout the whole energy dimension: from thermal particles to high-energy particles. Quasi-linear theory over-predicts the fluxes by about 15%; however, this reasonable agreement is the result of a compensation between two larger errors of about 50%, both at the resonant energy and at the thermal energy. *Published by AIP Publishing.*

<https://doi.org/10.1063/1.5057420>

I. INTRODUCTION

Understanding and being able to predict core turbulent (or anomalous) transport, in order to mitigate it, is crucial to achieve controlled fusion energy.

Turbulence appears spontaneously in strongly magnetized plasmas from microinstabilities driven by density, temperature, and sometimes velocity gradients.¹ Turbulence is a highly nonlinear process involving multi-scale phenomena in phase space and time.² Indeed plasma microinstabilities can give rise to large scale structures such as zonal flows^{3–6} or streamers.^{7–9}

This multi-scale physics is particularly challenging for numerical computation. In essence, the nonlinearity of the turbulence is described by a system consisting of a Vlasov (or collisionless Boltzmann) equation for each species coupled to Maxwell equations. The solution of the Vlasov equation for a species s is the distribution function $f_s(\vec{r}, \vec{v}, t)$ depending of the time t and a 6 dimensional phase space (\vec{r}, \vec{v}) .

Gyrokinetic theory allows one to reduce the dimensionality from 6 to 5 (by averaging out the fast cyclotron motion). The resulting phase-space is 4D (3 gyro-center spatial coordinates, plus the guiding center parallel velocity \bar{v}_{\parallel}), parametrized by the magnetic moment $\bar{\mu}$ which is an invariant.^{1,10,11}

When considering low frequency turbulence, typically on the order of the trapped particles toroidal precession frequency, it is then possible to average out the bounce motion, furthermore reducing the dynamics to a reduced 2D phase-space, parametrized by the energy and pitch-angle invariants, thus saving CPU time. The TERESA code used in this paper is based on this reduced model and solves the Vlasov-Poisson system^{12–14} using a Semi-Lagrangian numerical scheme.^{1,15,16}

Exploring the details of the velocity space with brute force gyrokinetic simulation, even with a local code, can consume up to 10^8 core hours on a modern supercomputer.¹⁷ The global gyro-bounce averaged code TERESA allows one to study the details of the trapped particle dynamics in the velocity space, without degrading the precision in the real space and at reasonable numerical cost.

For collisionless trapped-particle-driven modes, such as the trapped-electron mode (TEM) or the trapped-ion mode (TIM), we expect the mode-particle resonance to play an essential role in the particles and heat fluxes. It was found recently that this poses an issue for the accuracy required to describe the mode structure, which has a strong, narrow peak around the resonant energy.¹⁸ Trapped-ion modes being weakly dispersive, all resonances in the turbulent case could be very localized in the velocity (or energy) space. This raises the issue of the precision required to accurately describe the fluxes in the velocity space in gyrokinetic simulation when weakly dispersive modes are present. Usually, conventional gyrokinetic simulation focuses on the fine description of the real space but is limited to only a handful of points in the velocity dimensions.

The present work aims to describe in detail the velocity dependence of the heat and density radial fluxes in nonlinear simulations from the gyro-bounce averaged code TERESA, in order to give an estimate of the accuracy required in the velocity space to describe the resonant fluxes. In this article, we focus on trapped-ion modes although TERESA can treat TEM as well.

To provide some reference point, the results from TERESA's nonlinear simulation will be compared with the

quasi-linear theory. More than five decades after the two pioneering papers,^{19,20} quasi-linear theory^{21–23} is still relevant because in spite of *a priori* crude simplifications, its estimations of turbulent fluxes remains in good agreement with experimental results^{24,25} as well as with nonlinear gyrokinetic simulations.^{26,27}

The principal assumptions of the quasi-linear theory are a low level of fluctuations of the distribution function (i.e., $f = f_{eq} + \delta f$ and $|\delta f| \ll f_{eq}$, where f_{eq} describes a slowly evolving background distribution that is changing due to the effects of the unstable waves themselves) and that there is no trapped particle inside “potential wells.”^{19,28} These assumptions can be questioned in the case of trapped particle driven modes, where wave/particle resonances play a central role. Quasi-linear theory also relies upon the assumption that the correlation time τ_C of the electric field seen by a resonant particle is small as compared to the evolution time of averaged quantities.²⁹

We describe the gyro-bounce averaged model of TERESA in Sec. II. In Sec. III, we give the simulation configuration and input parameters. In Sec. IV, we show the radial density and heat flux from the TERESA simulation in the real space (ψ , corresponding to the minor radius), then we separate the contribution to the heat flux from thermal (low energy) particles and resonant particles. We also introduce quasi-linear theory with the purpose to give an element of comparison for the fluxes. Then, in Sec. V, we explore in detail the energy dependence of the radial particle flux from TERESA, and we compare it to the quasi-linear estimation.

II. MODEL-TERESA CODE

The TERESA (Trapped Element REduction in Semi Lagrangian Approach) code is based on an electrostatic reduced bounce-averaged gyrokinetic model.^{12,14,30} The dynamics considered is on the order of the trapped particle precession timescale. Averaging out the cyclotron and bounce motions allows one to reduce the dimensionality from 6D to 4D. The bounce-averaged distribution function f of the trapped particles (or “banana center”) thus depends on 2 phase-space variables (an angle and an action) and 2 invariants. The phase-space variables are the poloidal magnetic flux ψ which is a function of the minor radius and will be used as a radial coordinate for the numerical simulations, and an angle $\alpha = \varphi - q\theta$ which is the toroidal precession angle, where φ is the toroidal angle, q is the safety factor, and θ is the poloidal angle. The phase space is parametrized by 2 invariants: the particle kinetic energy E and the trapping parameter $\kappa = \sqrt{\frac{1-\lambda}{2\epsilon\lambda}}$, where $\lambda = \frac{\mu B_{min}}{E}$, μ is the magnetic moment, B_{min} is the minimum magnetic field amplitude, and $\epsilon = \frac{a}{R_0}$ is the inverse aspect ratio (a being the minor radius and R_0 the major radius at the magnetic axis).

The passing particle dynamics is considered adiabatic. In this article, we focus on the trapped ion dynamics and a quasi-adiabatic response of electrons is assumed although the model allows kinetic response of both ions and electrons. The time evolution of the bounce-averaged distribution function f of the trapped ions (or “banana center”) is determined by the Vlasov equation

$$\frac{\partial f}{\partial t} - [\mathcal{J}_0 \phi, f]_{\alpha, \psi} + E \Omega_d \frac{\partial f}{\partial \alpha} = 0, \quad (1)$$

where ϕ is the plasma electrostatic potential, $E \Omega_d$ is the energy-dependent precession frequency, $[g, h]_{\alpha, \psi} = \partial_\alpha g \partial_\psi h - \partial_\alpha h \partial_\psi g$ are the Poisson bracket, and \mathcal{J}_0 is the gyro-bounce-averaging operator.

Equation (2) is obtained from the Poisson equation; it closes the system and allows the model to be self-consistent

$$\begin{aligned} C_1 \left[\phi - \langle \phi \rangle_\alpha + \mathcal{F}^{-1} \left(i \delta_m \hat{\phi}_m \right) \right] - C_2 \bar{\Delta} \phi \\ = \frac{2}{\sqrt{\pi}} \int_0^\infty \mathcal{J}_0(E) f \sqrt{E} dE - 1, \end{aligned} \quad (2)$$

where \mathcal{F}^{-1} is the inverse Fourier transform, δ_m is the electron dissipation which takes into account the effects of electron-ion collisions, expressed as a phase-shift between electron density and perturbed electric potential,¹⁸ and $\hat{\phi}_m$ is the m th component of the Fourier decomposition in α of ϕ . $C_1 = C_2(1 - f_T)(1 + \tau)/f_T$ and $C_2 = a/R_0$ are dimensionless, constant input parameters, where f_T is the fraction of trapped particles and τ is the ion/electron temperature ratio, and $\bar{\Delta} \phi$ is the polarization term of the quasi-neutrality equation, with $\bar{\Delta} = \left(\frac{q_0 \rho_0}{a} \right)^2 \frac{\partial^2}{\partial x^2} + \delta_b^2 \frac{\partial^2}{\partial \psi^2}$.

This reduced model relies on the following assumptions:

- The equilibrium configuration is that of a large aspect ratio tokamak. However, the inverse aspect ratio ϵ must not be so small that the fraction $f_T \sim \sqrt{\epsilon}$ of trapped particles is negligible.
- Resonant interactions are dominated by strongly trapped ions. In this case, we can neglect the radial variation of precession frequency, and we focus on a single value of the pitch-angle.
- The mode frequency is much lower than the passing ion transit frequency.
- The plasma is at low- β , in other words trapped ion precession resonance-driven modes are mostly electrostatic.

All the physical quantities are normalized as listed in Table I. We will now omit the hat for normalized quantities for clarity.

More details on this model are available in Refs. 12–14 and 30–33.

III. SIMULATION CONFIGURATION

We run our nonlinear simulations with the gyrokinetic code TERESA and we focus on the ion dynamics. The grid in phase space is uniform, with N_ψ points in $\psi \in [0; 1]$, with $\psi = 1$ being in the center of the fusion plasma and $\psi = 0$ being toward the edge (but still in the core) and N_α points in the toroidal precession angle $\alpha \in [0; 2\pi[$. We choose $N_\alpha \times N_\psi = 256 \times 257$. For the 2 invariants, the grid has N_E points in $E \in [0; 20]$. It should be noted that such a range of energy is required for the convergence of the simulation results. A single value in $\kappa = 0$ which corresponds to deeply trapped particles¹³ is chosen. The energy grid is finer close to $E = 0$ and looser for higher E allowing greater precision

TABLE I. Normalization. Physical quantities are noted without a hat, and dimensionless quantities with a hat. Here, $\omega_{d,0} \equiv q_0 T_0 / (eaR_0 B_0)$ is a typical precession frequency of strongly trapped ions at $E = T_0$, n_0 and T_0 are arbitrary normalizing ion density and temperature such that $\hat{n} = \hat{T} = 1$ at $\hat{\psi} = 1$, and $L_\psi = a^2 B_0 / q_0$ is the radial size of the simulation box in magnetic flux units. Note that the minor radius a , the Larmor radius ρ_0 , and the banana width δ_b are all expressed in units of Ψ here. In the main text, the notation “” is omitted for clarity.

Dimension of	e.g.	Normalization
Time	t, ω^{-1}	$\hat{t} = \omega_{d,0} t$
Length	r	$\hat{r} = r(B_0/q_0 L_\psi)^{1/2}$
Poloidal magnetic flux	$\psi, a, \rho_0, \delta_b$	$\hat{\psi} = \psi / L_\psi$
Electric potential perturbation	ϕ	$\hat{\phi} = (R_0/a) e\phi / T_0$
Energy	E	$\hat{E} = E / T_0$
Density	n	$\hat{n} = n / n_0$
Temperature	T	$\hat{T} = T / T_0$

for low E . This is done using a new parameter $V = \sqrt{E}$ instead of the parameter E itself, so that the new grid in V still has N_E points but is finer in terms of E for low V , corresponding to low E . In this paper, we choose $N_E = 1024$. We noticed, for instance, an error of about 6% on the density and heat fluxes when we choose 128 points in energy instead of 1024 points. With 64 points in energy, the density flux has an error of 25% and the heat flux an error of 10%.

Here, the TERESA simulations are performed with thermal baths at both outside boundary $\psi = 0$ and inside boundary $\psi = 1$. Artificial dissipation is imposed in buffer regions $\psi < 0.15$ and $\psi > 0.85$ to smooth out the transition between turbulent fluctuations of ϕ , and the constraint $\phi = 0$ at $\psi = 0$ and $\psi = 1$. In the figures represented with a ψ axis, the buffer zones are for $\psi \in [0; 0.15]$ and $\psi \in [0.85; 1]$, and will be shaded in grey.

We choose the ion Larmor radius $\rho_i = 0.01$ and the ion banana width $\delta_{bi} = 0.1$.

The initial radial temperature gradient is $\kappa_T = 0.15$.

At $t = 0$, the electrostatic potential is a sum of sines both in α and ψ , multiplied by an envelope, so that it is close to zero at $\psi = 0$ and $\psi = 1$, and writes

$$\phi|_{t=0} = \phi_{\text{sum of sines}} \left(\tanh\left(\frac{\psi - \psi_2}{L_\psi}\right) + \tanh\left(\frac{L_\psi - \psi - \psi_2}{L_\psi}\right) \right), \quad (3)$$

where $\psi_2 = 0.15$ and $L_\psi = 1$.

The buffers artificial diffusion is of the form

$$D_{\text{buffers}}(\psi) = D_0 \left[2 - \left(\tanh\left(\frac{\psi - \psi_0}{L_D}\right) + \tanh\left(\frac{L_\psi - \psi_0 - \psi}{L_D}\right) \right) \right], \quad (4)$$

with $D_0 = 0.001$, $\psi_0 = 0.1$, and $L_D = 0.02$.

The equilibrium distribution function f_{eq} is chosen as locally Maxwellian in V (so exponential in E) as

$$f_{eq}(\psi, E) = e^{-E} [1 + (\kappa_T(E - 3/2) + \kappa_n)\psi], \quad (5)$$

TABLE II. Grid used for our simulations. α and ψ are the phase-space variables while κ and E (or V) are parameters.

Grid	Number of grid points	Value
α	$N_\alpha = 256$	$\alpha \in [0; 2\pi[$
ψ	$N_\psi = 257$	$\psi \in [0; 1]$
κ	$N_\kappa = 1$	$\kappa = 0$
E, V	N_E or $N_V = 1024$	$E \in [0; 20]$

where $\kappa_n \equiv \frac{\partial \log(n_{eq})}{\partial \psi} \Big|_{\psi=0}$ is a constant input parameter, which measures the equilibrium density gradient and similarly κ_T measures the temperature gradient.

The grid configuration and the input parameters are recalled in Tables II and III, respectively.

IV. TRAPPED-ION-MODE TURBULENCE AND RADIAL TRANSPORT

In this section, we analyse the evolution of the turbulent field, and the resulting density and heat fluxes obtained from the TERESA simulation.

A. Time evolution of dominant modes

Figure 1 shows the obtained time evolution of a selection of dominant modes. We observe a phase of linear growth of the plasma potential from $t = 0$ until $t \approx 4-5$. Linearly, the most unstable mode is the mode number $l = 9$, where $\phi = \sum_l \phi_l \exp(il\alpha)$. Its linear frequency and growth rate are $\omega_l = 15.6$ and $\gamma_l = 0.987$. After $t = 5$, the modes achieve their saturation level. The saturation amplitude in terms of the root mean square ϕ_{rms} is on the order of $\phi_{rms} \sim 0.05$. In physical units, since we have chosen an aspect ratio $\epsilon = 0.1$, we obtain $e\phi_{rms}/T \sim 5 \times 10^{-3}$.

At $t \approx 5$, the most intense modes are the modes around $l = 10$. For the rest of this article, we investigate the time $t = 5$, at the beginning of the turbulent phase, where the dominant modes have just achieved saturation.

B. Particle, density, and heat fluxes

Averaging the Vlasov equation over the angle α yields

$$\frac{\partial \langle f \rangle_\alpha}{\partial t} = \frac{\partial}{\partial \psi} \Lambda_\psi^{\text{NL}}(\psi, E, t), \quad (6)$$

with

TABLE III. Input parameters.

Quantity	Value
Ion Larmor radius	$\rho_i = 0.01$
Ion banana width	$\delta_{bi} = 0.1$
Initial temperature gradient	$\kappa_T = 0.15$
Initial density gradient	$\kappa_n = 0$
Trapped particle precession frequency	$\Omega_d = 1$
C1	$C_1 = 0.1$
C2	$C_2 = 0.1$
Electron dissipation ¹⁸	$\delta_m = 0.02$

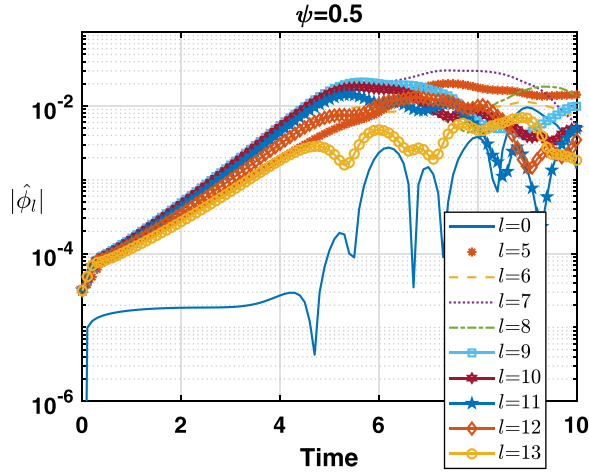


FIG. 1. Time-evolution of the amplitude of 10 Fourier modes of the electric potential ϕ . The modes $l=5$ to $l=13$ correspond to the 9 most intense modes and the $l=0$ mode corresponding to the zonal flow. The intensity of each $l \neq 0$ mode grows in the linear phase from $t=0$ to $t \approx 5$, when they reach saturation level. The dominant modes at time $t \approx 5$ are the modes 7, 8, 9, 10, and 11. This plot is for $\psi = 0.5$. For $\psi = 0.3$ or $\psi = 0.7$, the only significant difference is that the $l=0$ mode corresponding to the zonal flow has an intensity of the same order of magnitude as the other modes.

$$\Lambda_{\psi}^{\text{NL}}(\psi, E, t) = -\langle \dot{\psi} f \rangle_{\alpha} = \left\langle \frac{\partial \mathcal{J}_0 \phi}{\partial \alpha} \delta f \right\rangle_{\alpha}, \quad (7)$$

where $\delta f = f - \langle f \rangle_{\alpha}$.

The quantity $\Lambda_{\psi}^{\text{NL}}$ is the nonlinear radial particle flux. It is calculated directly within the TERESA simulation.

Taking the moments of Eq. (6) yields the following conservation equations:

$$\frac{\partial \langle n \rangle_{\alpha}}{\partial t} = \frac{\partial \Gamma^{\text{NL}}}{\partial \psi}, \quad (8)$$

$$\frac{\partial \langle nT \rangle_{\alpha}}{\partial t} = \frac{\partial q^{\text{NL}}}{\partial \psi}, \quad (9)$$

with the density flux

$$\Gamma^{\text{NL}}(\psi, t) = \int_E \Lambda_{\psi}^{\text{NL}}(\psi, E', t) \sqrt{E'} dE' \quad (10)$$

or the heat flux

$$q^{\text{NL}}(\psi, t) = \int_E \Lambda_{\psi}^{\text{NL}}(\psi, E', t) E' \sqrt{E'} dE'. \quad (11)$$

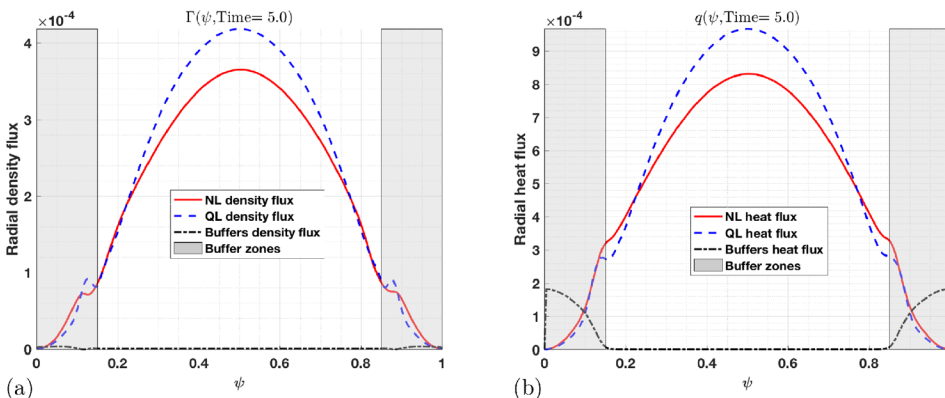


FIG. 2. Nonlinear and quasi-linear radial density (a) and heat (b) fluxes as a function of ψ and at $t=5$.

The velocity space is linked to the energy space as $d^3v = C\sqrt{E}dE$ with C being a constant,³⁴ (p. 44); therefore, we add a \sqrt{E} factor inside the integral over energy space to physically integrate over the velocities.

Note that we distinguish the particle (in the sense of “test particle”) flux Λ , which is also the flux of phase-space density, and the density (in the sense of fluid density) flux Γ .

Figure 2(a) shows the density flux $\Gamma(\psi, t)$, and Fig. 2(b) shows the heat flux $q(\psi, t)$, both at the given time $t=5$. The quasi-linear fluxes will be discussed later. The artificial density and heat fluxes due to the buffers diffusion in TERESA are included. The positive sign of both Γ and q is consistent with a flattening of the initial gradients. The fluxes are bell shaped because of the boundary conditions restraining the instability to a 0 value at $\psi=0$ and $\psi=1$. Simulation with larger box size yielded flatter flux profile, but with higher numerical cost, so this paper focuses on a “small box.”

In order to obtain more information about the origin of turbulent transport, we are now going to separate the contribution from thermal particles and from resonant particles, by integrating over different ranges of energy E .

Thermal particles and resonant particles will be discriminated as follows: thermal particles’ range of integration will be $E \in [0; 1.4]$ and for the resonant particles $E \in [1.4; 2.4]$.

These integration intervals are chosen to take into account all the particles below the resonance energy for the thermal particles and all the particles in the resonance peak for the resonant particles. These choices are coherent considering Figs. 4 and 5, discussed later in the paper.

Figures 3(a) and 3(b) show the contribution to the heat flux of the thermal and the resonant particles, respectively.

The resonant particles’ contribution accounts for more than 90% of the total heat flux. Furthermore, the contribution from thermal particles has the opposite sign. This can be simply explained by the sign of $\frac{\partial \langle f \rangle_{\alpha}}{\partial \psi}$ which is positive for $E > 3/2$ but negative for $E < 3/2$.

Here, we focused on heat, but similar conclusions are reached for the density flux.

C. Quasi-linear theory

Quasi-linear theory describes the slow evolution ($\frac{\partial \log \langle f \rangle}{\partial t} \ll \gamma_k$ with γ_k the linear growth rate of the most unstable mode) of the α -averaged particle distribution function $\langle f \rangle_{\alpha}$, as the solution of a diffusion equation³⁵

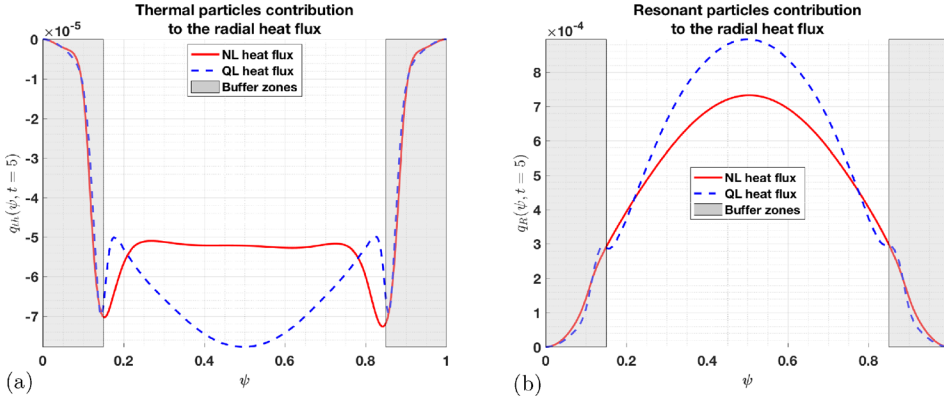


FIG. 3. (a) $q_{th}^{NL,QL}(\psi, t) = \int_{E_1=0}^{E_2=1.4} \langle \Lambda_{\psi}^{NL,QL} \rangle_{\alpha}(\psi, E', t) E' \sqrt{E'} dE'$ takes into account only the thermal particles contribution to the heat flux. (b) $q_R^{NL,QL}(\psi, t) = \int_{E_2=1.4}^{E_3=2.4} \langle \Lambda_{\psi}^{NL,QL} \rangle_{\alpha}(\psi, E', t) E' \sqrt{E'} dE'$ takes into account only the resonant particles contribution to the heat flux. The buffer zones are shaded.

$$\frac{\partial \langle f \rangle_{\alpha}}{\partial t} = \frac{\partial}{\partial \psi} \left(D_{QL} \frac{\partial \langle f \rangle_{\alpha}}{\partial \psi} \right). \quad (12)$$

In other words, the particle flux takes a specific form $\Lambda_{\psi}^{QL}(\psi, E, t) = D_{QL} \frac{\partial \langle f \rangle_{\alpha}}{\partial \psi}$.

Equation (12) is obtained by substituting the linear response for ϕ and δf in Eq. (7), which implies neglecting some of the nonlinear coupling terms as described in [Appendixes A and B](#).

The main hypotheses of quasi-linear theory are weak turbulence (small fluctuations of the profiles compared to the equilibrium), no trapped particles in electrostatic potential “wells” (with a very large number of electrostatic waves, the resonance region of each waves can overlap so that the particle motion becomes stochastic, and the particle can wander in the velocity phase space^{35,36}), and a small auto-correlation time of the electric field compared to the evolution time of the profiles.

The quasi-linear radial particle flux $\Lambda_{\psi}^{QL}(\psi, E, t)$ is the product of the quasi-linear diffusion coefficient D_{QL} and the mean gradient

$$\Lambda_{\psi}^{QL}(\psi, E, t) = -D_{QL}(\psi, E, t) \frac{\partial \langle f \rangle_{\alpha}}{\partial \psi}(\psi, E, t), \quad (13)$$

with

$$D_{QL}(\psi, E, t) = \sum_l l^2 |\hat{\phi}_l(\psi, E, t)|^2 \frac{1 - e^{-i(\omega_{R,l} - \omega_l)t - \gamma_l t}}{i(\omega_{R,l} - \omega_l) + \gamma_l}, \quad (14)$$

and

$$\omega_{R,l}(\psi, E, t) = l \left(\frac{\Omega_d E}{Z} + \frac{\partial \hat{\phi}_0}{\partial \psi} \right), \quad (15)$$

where the sum \sum_l is over the l components of the Fourier decomposition in α of the gyro-bounce averaged electrostatic potential, noted $\hat{\phi}_l(\psi, E, t)$. Derivation of Eqs. (13) and (14) is detailed in [Appendix A](#). γ_l and ω_l are, respectively, the growth rate and linear frequency of each trapped-ion mode l , $\omega_{R,l}(\psi, E, t)$ is homogeneous to a frequency and $\frac{\partial \hat{\phi}_0}{\partial \psi}$ accounts for the Doppler effect from the mean flow (including zonal flow), and the trapped particles’ precession frequency Ω_d and Z are equal to 1 in our normalized units.

The moments of Eq. (13) yield the QL density flux

$$\Gamma^{QL}(\psi, t) = \int_E \Lambda_{\psi}^{QL}(\psi, E', t) \sqrt{E'} dE' \quad (16)$$

or the QL heat flux

$$q^{QL}(\psi, t) = \int_E \Lambda_{\psi}^{QL}(\psi, E', t) E' \sqrt{E'} dE'. \quad (17)$$

To compute the quasi-linear fluxes, the electrostatic potential ϕ , the mean distribution function $\langle f \rangle_{\alpha}$, the modes growth rate γ_l , and the modes frequency ω_l are needed.

In order to test fundamental aspects of the QL formalism, we want to limit the sources of discrepancies between QL theory and NL simulations. We thus take ϕ and $\langle f \rangle_{\alpha}$ directly from the TERESA simulation, instead of using approximations such as the mixing length. γ_l and ω_l are obtained from the resolution of the linear dispersion relation.^{14,33}

D_{QL} includes the contribution of the zonal flow. Because the zonal radial electric field $\frac{\partial \hat{\phi}_0}{\partial \psi}$ fluctuates rapidly in ψ and in time, which can create artifact in the resonance considering its presence in the denominator of Eq. (14), we average this quantity over time and ψ .

Considering we are only interested in the time $t = 5$, we thus perform a time averaging over $t \in [4.8; 5.2]$. This time window (0.4) corresponds to a typical oscillation time of $\frac{\partial \hat{\phi}_0}{\partial \psi}$. We then perform a moving average in ψ with a 100 points window. This window in ψ corresponds to approximately a third of the total box size in ψ .

After these averages, the quantity $\frac{\partial \hat{\phi}_0}{\partial \psi}$ has only a ψ dependence and can take positive or negative values. For example, for the highest oscillation amplitude of $\frac{\partial \hat{\phi}_0}{\partial \psi}$ we have $\frac{\partial \hat{\phi}_0}{\partial \psi}(\psi \approx 0.28) \approx 0.06$ and $\frac{\partial \hat{\phi}_0}{\partial \psi}(\psi \approx 0.34) \approx -0.05$. These oscillations in value have an impact on the position in energy of the resonance peak. Between these values of ψ , the resonance peak can shift in energy space from $E \approx 1.79$ to $E \approx 1.66$, only by considering two ψ positions yet quite close.

Figures 2 and 3 include the QL prediction for the density and heat fluxes. The NL fluxes and QL predictions are in qualitative agreement. However, there are significant quantitative discrepancies, even as we have chosen the best case scenario for QL theory (t not too large, ϕ and $\frac{\partial f}{\partial \psi}$ directly from simulation and no mixing length estimate). The quasi-linear estimation of the density flux, the heat flux, the thermal particles contribution to the heat flux, and the resonant

particle contribution to the heat flux, respectively, present a 16%, 16%, 50%, and a 20% discrepancy compared to the nonlinear flux obtained from the TERESA simulation. In [Appendix B](#), we present a comparison of the neglected or kept terms in the quasi-linear equation. We find that two key terms contribute to the radial transport: the linear term $\frac{\partial \phi}{\partial x} \frac{\partial \langle f \rangle}{\partial \psi}$ which is kept in the quasi-linear equation and the nonlinear term $\langle \frac{\partial \phi}{\partial x} \frac{\partial \delta f}{\partial \psi} \rangle$ which is neglected. A comparison term by term shows that the neglected nonlinear term which contributes to the radial transport is in fact greater than the kept linear term. This may explain the discrepancy between the nonlinear and quasi-linear fluxes.

Section [V](#) is focused on the investigation of the details in the velocity (or energy) space of these fluxes.

V. ANATOMY OF THE RADIAL FLUXES IN THE ENERGY SPACE

TERESA allows us to investigate in detail the velocity (or energy) space at reduced computational cost. In this section, we will investigate the energy dependence of the particle flux $\Lambda^{\text{NL}}(\psi, E, t)$, at $\psi = 0.5$ and at time $t = 5$, taking advantage of our large number of grid points in energy, $N_E = 1024$. In order to have some reference point, we will then compare Λ^{NL} to the quasi-linear particle flux Λ^{QL} .

The quasi-linear diffusion, Eq. (14), presents a resonance for each mode l , when $\omega_{R,l}(\psi, E_R, t) = \omega_l$, with $E_R = \frac{Z}{\Omega_d} \left(\frac{\omega_l}{l} - \frac{\partial \phi_0}{\partial \psi} \right)$. This peak is the result of the resonance between the low frequency trapped ions modes and the precession of trapped particles. The position of the resonance for each mode is mainly determined by the ratio $\frac{\omega_l}{l}$. The mean flow contribution $\frac{\partial \phi_0}{\partial \psi}$ slightly shifts the position of the resonance as discussed in [Sec. IV](#). The contribution of the most intense modes to the fluxes will be greater, so that the peak position will be mainly determined by these most intense modes at $t = 5$ (see [Fig. 1](#)). [Figure 4](#) shows the resonant energy E_R as a function of the modes l . The dominant modes ($l = 7-11$) have their resonant energy in the range

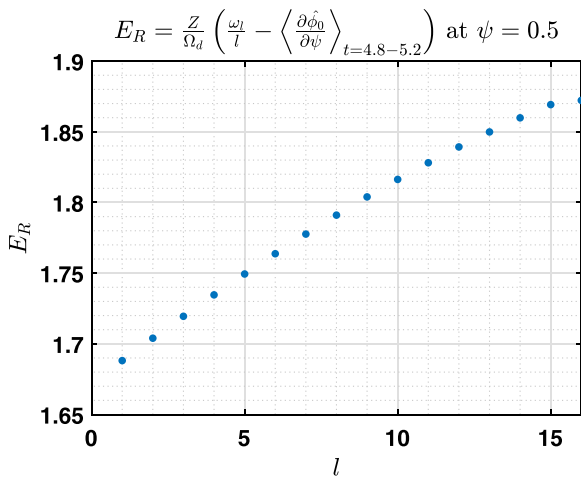


[FIG. 4](#). Resonance condition for each modes l with $\Omega_d = 1$ and $Z = 1$. The time averaging around $t = 5$ of $\frac{\partial \phi_0}{\partial \psi}$ is necessary and is explained in [Sec. IV](#). This figure, coupled with [Fig. 1](#), shows that we can expect the resonance to be the most intense for an energy $E \approx 1.78$ to $E \approx 1.83$ at $t = 5$, because the most intense modes in $\psi = 0.5$ are the modes between $l = 7$ and $l = 11$.

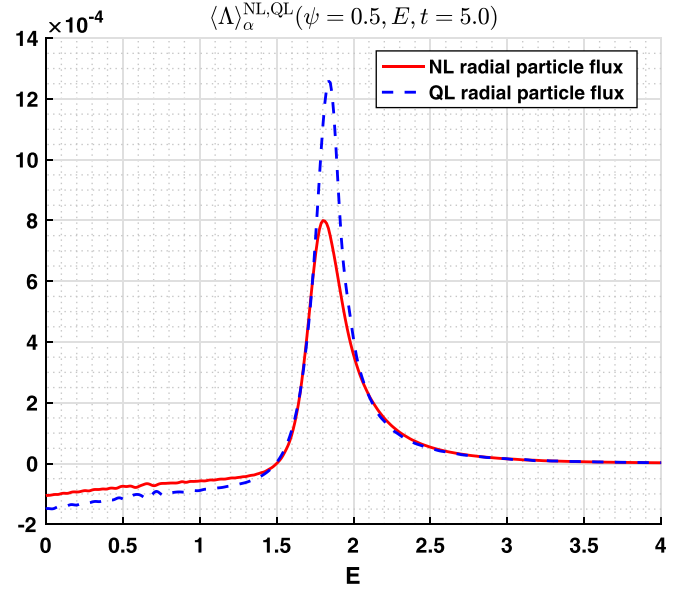


[FIG. 5](#). Nonlinear and quasi-linear radial particles fluxes as a function of E and at $t = 5$.

$E \in [1.78; 1.83]$. Therefore, we can expect a narrow, $\Delta E \approx 0.05$ resonance peak for the flux around $E \approx 1.8$.

[Figure 5](#) shows the particle flux (or flux of phase-space density f), $\Lambda^{\text{NL}}(\psi, E, t)$, at a fixed radius $\psi = 0.5$. The sign is everywhere consistent with a flattening in ψ of $\langle f \rangle_\alpha$ (since $\frac{\partial \langle f \rangle_\alpha}{\partial \psi}$ is negative for $E < 3/2$ and positive for $E > 3/2$, as explained in [Sec. IV B](#)). As expected, the nonlinear (from TERESA simulation) fluxes in the energy/velocity space, at the middle of the box and at $t = 5$, present a narrow resonance peak. The resonance peak width is about $\Delta E \approx 0.15$ (obtained by a Gaussian fit of the resonance peak, $\Lambda^{\text{NL}} \sim \exp[(E - E_0)/\Delta E]$). Strikingly, the resonance peak accounts for most of the flux. Indeed, the flux at the resonance is one order of magnitude stronger than the flux for thermal particles, while the high energy particle flux tends to 0.

We must keep in mind that the position of this resonance peak is determined by the most intense electrostatic modes at this ψ and time and can be slightly shifted by the intensity of the zonal radial electric field $\frac{\partial \phi_0}{\partial \psi}$.

[Figure 5](#) includes the QL particle flux Λ^{QL} as well. The NL and QL fluxes are in qualitative agreement, in terms of sign, energy of sign reversal, position of peak, width of peak, and behavior at large energies. However, quantitatively, the discrepancy between the nonlinear fluxes and the quasi-linear estimation is of 41% at $E = 0$, 55% at $E = 1$, and 57% at the resonance peak. As discussed in [Sec. IV C](#), [Appendix B](#) shows that out of two terms contributing to the radial transport, only the linear term is kept in the quasi-linear theory, while the nonlinear term is neglected. The term by term comparison shows that the neglected nonlinear term is greater than the kept linear term, which may explain this discrepancy.

VI. CONCLUSION

We performed a numerical simulation of trapped ion mode turbulence with the bounce-averaged gyrokinetic TERESA code. It is based on a reduced model, which is

meant to investigate fundamental mechanisms and trends, rather than provide realistic quantitative predictions for tokamaks. The trapped ions are treated kinetically, while the passing ions respond adiabatically. The electrons respond quasi-adiabatically. The simulation parameters correspond to a small aspect ratio (0.1), a radial box size of 10 banana widths, a flat density profile, and a moderate temperature gradient (gradient length of 67 banana widths). The electric potential in terms of root mean square ϕ_{rms} saturates to a value $e\phi_{rms}/T_0 \approx 5 \times 10^{-3}$.

To investigate how the radial turbulent transport depends on the energy dimension, the simulation was performed with a large number of grid points $N_E = 1024$. We focused on a radial location in the middle of the simulation box and on a time in the simulation where the dominant trapped-ion modes have just achieved saturation, corresponding to the beginning of the turbulent phase. As expected, the radial flux is negative for $E/T_0 < 3/2$ and positive for $E/T_0 > 3/2$, consistent with a flattening of the radial gradient of the distribution function. We emphasize that the flux features a narrow peak in the resonant region, with a width $\Delta E/T_0 \approx 0.15$, around the energy $E/T_0 \approx 1.8$. Strikingly, this resonant peak accounts for 90% of the density and heat fluxes. In contrast, the contribution from thermal particles is negligible. Based on these results, a fine mesh in the energy space ($\delta E \ll 0.1T_0$), in the resonant region, is required to accurately describe the radial transport of density and heat.

The quasilinear predictions for radial fluxes (including the effect of zonal flow) are in qualitative agreement with the simulation results, in terms of global structure in the radial direction, sign throughout the energy dimension, behavior at small and large energies, and for the resonant peak in terms of its shape, location, and width in the energy dimension. However, quantitatively, there is a 57% overprediction at the peak, and a 55% overprediction at the thermal energy $E = T_0$. Since the flux is positive for resonant energies, and negative for thermal energies, these discrepancies can compensate each other. Indeed, the total density and heat fluxes predicted by quasi-linear theory are in good quantitative agreement with the nonlinear simulation result, with only 16% overprediction. However, this agreement is only a result of compensating errors. We showed that the non-zonal nonlinear part of the radial advection in the Vlasov equation is actually slightly larger than the linear part. This can explain the discrepancy since quasi-linear theory discards the non-zonal nonlinear part to obtain the response of the perturbed distribution function $f - \langle f \rangle$. Here, we should emphasize that we have chosen to maximize the chances of success of quasilinear theory. Indeed, both electric potential and mean distribution were taken directly from the nonlinear simulation and substituted into the quasilinear formula for the flux. We did not use theory-based assumptions for the potential spectrum and amplitude nor did we use an analytic equilibrium for the mean distribution. In this sense, we did not really test a prediction, but rather we have tested the assumptions underlying quasilinear theory.

In this paper, we focused on the trapped ion mode (TIM), but we expect similar results for the trapped electron mode (TEM). However, our analysis does not include the

effects of neither ion-temperature-gradient (ITG) nor electron-temperature-gradient (ETG) modes since the kinetic description in TERESA is limited to trapped particles. We believe this is the main caveat to our analysis, since, for example, in ITG turbulence, resonances may not play such a crucial role in the transport, and therefore, the co-existence and/or the coupling between TEM and ITG may mitigate the importance of the resonant peak in the radial fluxes.

Another important caveat is that boundary conditions consist of thermal baths, which strongly restrict the evolution of the profiles. As a result, the heat flux remains small, and the relaxation of the initial temperature gradient is only marginal. A future analysis based on flux-driven simulations may provide new information about the role of resonant particles in turbulent transport.

ACKNOWLEDGMENTS

This work was granted access to the HPC resources of IDRIS under the allocation 2017-27862 made by GENCI (Grand Equipement National de Calcul Intensif).

This work was carried out within the framework of the EUROfusion Consortium and French Research Federation for Fusion Studies and received funding from the Euratom research and training programme 2014–2018 under Grant Agreement No. 633053. The views and opinions expressed herein do not necessarily reflect those of the European Commission.

APPENDIX A: QUASI-LINEAR DIFFUSION COEFFICIENT

In this appendix, the quasi-linear diffusion coefficient derivation for the TERESA model is detailed and adopted from the procedure developed in the case of the 1D Vlasov-Poisson model³⁶

The starting point is the Vlasov equation in normalized units

$$\frac{\partial f}{\partial t} + \left[\frac{E\Omega_d}{Z} + \frac{\partial \phi}{\partial \psi} \right] \frac{\partial f}{\partial \alpha} - \frac{\partial \phi}{\partial \alpha} \frac{\partial f}{\partial \psi} = 0, \quad (\text{A1})$$

where $f(\alpha, \psi, E, t)$ is the distribution of banana centers, Z is the charge number, and $\phi(\alpha, \psi, E, t) = \mathcal{J}_0(E)\bar{\phi}(\alpha, \psi, t)$ denotes the gyrobounce-gyroaverage of the electric potential $\bar{\phi}$, with

$$\mathcal{J}_0(E) \approx \left(1 + \frac{\rho_0^2}{4} E \frac{\partial^2}{\partial \alpha^2} \right) \left(1 + \frac{\delta_b^2}{4} E \frac{\partial^2}{\partial \psi^2} \right), \quad (\text{A2})$$

which comes from the Taylor expansion of the product of two Bessel functions, $\mathcal{J}_0(k_\perp \rho_0)$ and $\mathcal{J}_0(k_\psi \delta_b)$, in the limit of long-wavelength where $k_\perp \rho_0 \ll 1$ and $k_\psi \delta_b \ll 1$.^{31,34}

We transform f and ϕ in Fourier space in the α direction

$$\hat{f}_m(\psi, E, t) = \frac{1}{2\pi} \int_0^{2\pi} f e^{-im\alpha} d\alpha, \quad (\text{A3})$$

$$\hat{\phi}_m(\psi, E, t) = \frac{1}{2\pi} \int_0^{2\pi} \phi e^{-im\alpha} d\alpha. \quad (\text{A4})$$

The Fourier transform of Eq. (A1) yields

$$\begin{aligned} \frac{\partial \hat{f}_m}{\partial t} + im \frac{E\Omega_d}{Z} \hat{f}_m - im \hat{\phi}_m \frac{\partial \hat{f}_0}{\partial \psi} \\ = - \sum_l i l \hat{f}_l \frac{\partial \hat{\phi}_{m-l}}{\partial \psi} + \sum_{l \neq 0} i(m-l) \hat{\phi}_{m-l} \frac{\partial \hat{f}_l}{\partial \psi}. \end{aligned} \quad (\text{A5})$$

The rhs corresponds to nonlinear wave-wave and wave-particle interactions. In the framework of quasilinear theory, the nonlinear wave-wave and wave-particle interactions are assumed to be weak according to the hypotheses of weak turbulence and of no particle trapped in electrostatic potential. Thus, we neglect these nonlinear interactions except for $m=0$ or $l=m$. Therefore, for $m \neq 0$, Eq. (A5) is approximated by

$$\frac{\partial \hat{f}_m}{\partial t} + im \frac{E\Omega_d}{Z} \hat{f}_m - im \hat{\phi}_m \frac{\partial \langle f \rangle}{\partial \psi} + im \hat{f}_m \frac{\partial \hat{\phi}_0}{\partial \psi} = 0, \quad (\text{A6})$$

where $\langle \rangle$ is the average in α .

The latter equation is of the form

$$L \hat{f}_m = g(\psi, E, t), \quad (\text{A7})$$

where L is the linear operator $L = \partial_t + i\omega_{R,m}(\psi, E, t)$, with

$$\omega_{R,m}(\psi, E, t) = m \left(\frac{\Omega_d E}{Z} + \frac{\partial \hat{\phi}_0}{\partial \psi} \right) \quad (\text{A8})$$

and $g = im \hat{\phi}_m \partial_\psi \langle f \rangle$. For $\omega_{R,m} = 0$, the solution is trivial. For $\omega_{R,m} \neq 0$, Eq. (A7) can be solved using Green's function $G_E(t, s) = \exp[i\omega_{R,m}(s-t)]$, which is such that $LG_E = \delta(s-t)$. The solution is

$$\hat{f}_m(\psi, E, t) = \int_0^t e^{i\omega_{R,m}(s-t)} im \hat{\phi}_m(\psi, E, s) \frac{\partial \langle f \rangle}{\partial \psi}(\psi, E, s) ds. \quad (\text{A9})$$

It turns out that the latter expression is also valid for $\omega_{R,l}$.

Each mode is assumed to have a fixed frequency ω_m (obtained from linear theory), and a time-dependent growth rate γ_m

$$\hat{\phi}_m(\psi, E, t) = \hat{\phi}_m(\psi, E, 0) \exp \left[\int_0^t (-i\omega_m + \gamma_m(t')) dt' \right]. \quad (\text{A10})$$

For $m=0$, Eq. (A5) simplifies as

$$\frac{\partial \langle f \rangle}{\partial t} + \sum_l il \frac{\partial (\hat{f}_l \hat{\phi}_l^*)}{\partial \psi} = 0. \quad (\text{A11})$$

Substituting Eqs. (A9) and (A10) yields

$$\begin{aligned} \frac{\partial \langle f \rangle}{\partial t} = \frac{\partial}{\partial \psi} \left[\sum_l l^2 |\hat{\phi}_l(\psi, E, t)|^2 \int_0^t e^{i(\omega_{R,l} - \omega_l)(s-t)} \frac{\partial \langle f \rangle}{\partial \psi} \Big|_s \right. \\ \left. \times \exp \left(\int_t^s \gamma(t') dt' \right) ds \right]. \end{aligned} \quad (\text{A12})$$

Since the rhs phase-mixes for $t-s$ larger than a typical growth time γ^{-1} and a typical timescale of relaxation of $\langle f \rangle$, we can approximate $\int_t^s \gamma(t') dt'$ by $\gamma(t)(s-t)$ and $\partial_\psi \langle f \rangle|_s$ by $\partial_\psi \langle f \rangle|_t$. With this approximation, the time evolution of the α -averaged distribution function simplifies to

$$\frac{\partial \langle f \rangle}{\partial t} = \frac{\partial}{\partial \psi} \left[D_{\text{QL}} \frac{\partial \langle f \rangle}{\partial \psi} \right], \quad (\text{A13})$$

with

$$D_{\text{QL}}(\psi, E, t) = \sum_l l^2 |\hat{\phi}_l(\psi, E, t)|^2 \frac{1 - e^{-i(\omega_{R,l} - \omega_l)t - \gamma_l t}}{i(\omega_{R,l} - \omega_l) + \gamma_l}. \quad (\text{A14})$$

The electrostatic potential ϕ used will be the one obtained from the TERESA simulation.

The quasi-linear particle flux is, thus, the product of the quasi-linear diffusion coefficient D_{QL} and the α -averaged trapped ion distribution function gradient

$$\langle \Lambda_\psi \rangle_\alpha^{\text{QL}}(\psi, E, t) = -D_{\text{QL}}(\psi, E, t) \frac{\partial \langle f \rangle_\alpha}{\partial \psi}(\psi, E, t), \quad (\text{A15})$$

APPENDIX B: SYSTEM EQUATION TERMS COMPARISON

Quasi-linear theory neglects some of the nonlinear terms in the Vlasov-Poisson system.

In this appendix, we give details about the neglected or kept linear or nonlinear terms in the quasi-linear approximation.

The linear terms from Eq. (A5) are

- $L_{1,m} = \frac{\partial \hat{f}_m}{\partial t}$,
- $L_{2,m} = m E \hat{f}_m$,
- $L_{3,m} = m \hat{\phi}_m \frac{\partial \hat{f}_0}{\partial \psi}$

and the nonlinear terms are

- $\text{NL}_{1,m} = m \hat{f}_m \frac{\partial \hat{\phi}_0}{\partial \psi}$,
- $\text{NL}_{2,m} = \sum_{l \neq m} l \hat{f}_l \frac{\partial \hat{\phi}_{m-l}}{\partial \psi}$,
- $\text{NL}_{3,m} = \sum_{l \neq 0} (m-l) \hat{\phi}_{m-l} \frac{\partial \hat{f}_l}{\partial \psi}$.

In order to compare their magnitude, we take their absolute value and sum them over all non-zonal modes, which gives us the terms L_1 , L_2 , L_3 , NL_1 , NL_2 , and NL_3 , where

$$L_1 = \sum_{m \neq 0} |L_{1,m}|. \quad (\text{B1})$$

The terms kept in the quasi-linear equations are the terms $L_{1,2,3}$ and NL_1 .

We plot on Fig. 6 the linear and nonlinear terms of the system at a time $t=5$ of the simulation and as a function of the particles' energy.

L_1 is not represented because choosing an adequate timestep in order to evaluate $\frac{\partial \hat{f}_m}{\partial t}$ can be a tricky task considering the timestep taken for the simulation. However, it is possible to estimate the magnitude of this term.

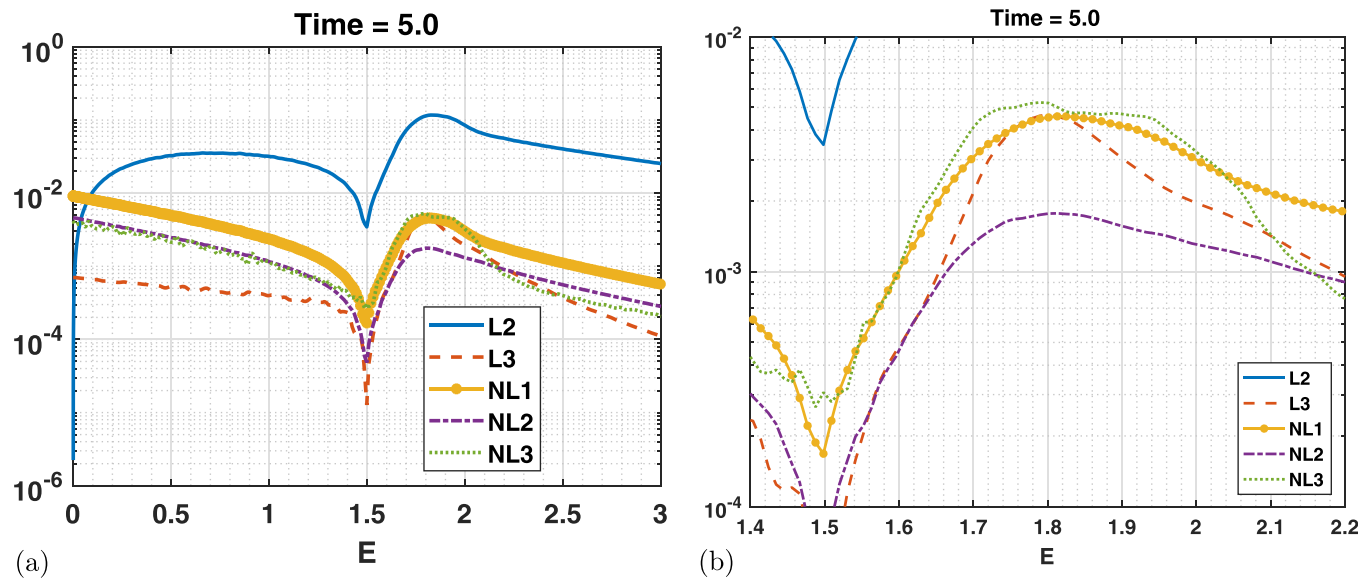


FIG. 6. (a) Comparison between linear and nonlinear terms from the system equations. In the quasi-linear theory the nonlinear coupling is neglected. (b) Zoom around the resonance on the key terms contributing to radial transport: L_3 and NL_3 .

From A5, we have $L_1 + L_2 + L_3 = NL_1 + NL_2 + NL_3$. We observe on Fig. 6 that $L_2 \gg L_3, NL_1, NL_2, NL_3$ (except for $E \ll 1$); thus, we deduce that L_1 is of the same order of magnitude as L_2 and that the two terms cancel each other out.

L_2 corresponds to the bananas precession around the toroidal direction and does not impact transport in the radial direction nor the QL radial fluxes.

L_3 contributes directly to the radial QL fluxes since it involves the gradient of $\langle f \rangle_\alpha$ in the ψ direction.

NL_1 involves the zonal radial electric field $\frac{\partial \hat{\phi}_0}{\partial \psi}$ and is the one responsible for the resonance peak shift in the energy/velocity dimension.

NL_2 and NL_3 correspond to all the other nonlinear couplings that do not involve the zonal flow. NL_3 contributes directly to the radial transport since it involves the gradient of $\langle f \rangle_\alpha$ in the ψ direction but is neglected in the framework of the quasi-linear theory.

The key terms influencing the radial fluxes are thus L_3 and NL_3 but only L_3 is taken into account.

We observe that the key term influencing the radial transport, kept in the quasi-linear theory (L_3), is small compared to the neglected nonlinear coupling term also influencing the radial transport (NL_3), especially around the resonance energy. The other neglected term (NL_2) is in contrast small compared to the other non-neglected terms. From this, one can expect large discrepancy between nonlinear and quasi-linear theory.

¹X. Garbet, Y. Idomura, L. Villard, and T. H. Watanabe, "Gyrokinetic simulations of turbulent transport," *Nucl. Fusion* 50(4), 043002 (2010).

²B. Borisovich Kadomtsev, *Plasma Turbulence* (Academic Press, 1965).

³Z. Lin, T. S. Hahm, W. W. Lee, W. M. Tang, and R. B. White, "Turbulent transport reduction by zonal flows: Massively parallel simulations," *Science* 281(5384), 1835–1837 (1998).

⁴B. N. Rogers, W. Dorland, and M. Kotschenreuther, "Generation and stability of zonal flows in ion-temperature-gradient mode turbulence," *Phys. Rev. Lett.* 85(25), 5336 (2000).

⁵E.-j. Kim and P. H. Diamond, "Dynamics of zonal flow saturation in strong collisionless drift wave turbulence," *Phys. Plasmas* 9(11), 4530–4539 (2002).

⁶P. H. Diamond, S. I. Itoh, K. Itoh, and T. S. Hahm, "Zonal flows in plasma: A review," *Plasma Phys. Controlled Fusion* 47(5), R35 (2005).

⁷A. M. Dimits, J. F. Drake, A. B. Hassam, and B. Meerson, "Formation of streamers in plasma with an ion temperature gradient," *Phys. Fluids B: Plasma Phys.* 2(11), 2591–2599 (1990).

⁸S. Champeaux and P. H. Diamond, "Streamer and zonal flow generation from envelope modulations in drift wave turbulence," *Phys. Lett. A* 288(3–4), 214–219 (2001).

⁹T. Yamada, S.-I. Itoh, T. Maruta, N. Kasuya, Y. Nagashima, S. Shinohara, K. Terasaka, M. Yagi, S. Inagaki, Y. Kawai *et al.*, "Anatomy of plasma turbulence," *Nat. Phys.* 4(9), 721 (2008).

¹⁰A. Brizard and T. Hahm, "Foundations of nonlinear gyrokinetic theory," *Rev. Mod. Phys.* 79(2), 421 (2007).

¹¹Y. Sarazin, V. Grandgirard, J. Abiteboul, S. Allfrey, X. Garbet, P. Ghendrih, G. Latu, A. Strugarek, and G. Dif-Pradalier, "Large scale dynamics in flux driven gyrokinetic turbulence," *Nucl. Fusion* 50(5), 054004 (2010).

¹²G. Depret, X. Garbet, P. Bertrand, and A. Ghizzo, "Trapped-ion driven turbulence in tokamak plasmas," *Plasma Phys. Controlled Fusion* 42(9), 949 (2000).

¹³T. Cartier-Michaud, P. Ghendrih, V. Grandgirard, and G. Latu, "Optimizing the parallel scheme of the Poisson solver for the reduced kinetic code Teresa," in *ESAIM: Proceedings* (EDP Sciences, 2013), Vol. 43, pp. 274–294.

¹⁴T. Drouot, E. Gravier, T. Reveille, A. Ghizzo, P. Bertrand, X. Garbet, Y. Sarazin, and T. Cartier-Michaud, "A gyro-kinetic model for trapped electron and ion modes," *Eur. Phys. J. D* 68(10), 280 (2014).

¹⁵E. Sonnendrücker, J. Roche, P. Bertrand, and A. Ghizzo, "The semi-Lagrangian method for the numerical resolution of the Vlasov equation," *J. Comput. Phys.* 149(2), 201–220 (1999).

¹⁶V. Grandgirard, M. Brunetti, P. Bertrand, N. Besse, X. Garbet, P. Ghendrih, G. Manfredi, Y. Sarazin, O. Sauter, E. Sonnendrücker *et al.*, "A drift-kinetic semi-Lagrangian 4d code for ion turbulence simulation," *J. Comput. Phys.* 217(2), 395–423 (2006).

¹⁷S. Maeyama, Y. Idomura, T.-H. Watanabe, M. Nakata, M. Yagi, N. Miyato, A. Ishizawa, and M. Nunami, "Cross-scale interactions between electron and ion scale turbulence in a tokamak plasma," *Phys. Rev. Lett.* 114(25), 255002 (2015).

¹⁸M. Lesur, T. Cartier-Michaud, T. Drouot, P. H. Diamond, Y. Kosuga, T. Reveille, E. Gravier, X. Garbet, S.-I. Itoh, and K. Itoh, "A simple model for electron dissipation in trapped ion turbulence," *Phys. Plasmas* 24(1), 012511 (2017).

¹⁹A. A. Vedenov, E. P. Velikhov, and R. Z. Sagdeev, "Quasi-linear theory of plasma oscillations," *Nucl. Fusion Suppl. Pt. 2*, 465 (1962).

- ²⁰W. E. Drummond and D. Pines, “Non-linear stability of plasma oscillations,” *Nucl. Fusion, Suppl. Pt. 3*, 1049–1057 (1962).
- ²¹J. C. Adam, G. Laval, and D. Pesme, “Effets des interactions résonnantes ondes-particules en turbulence faible des plasmas,” *Ann. Phys.* **6**, 319–420 (1981).
- ²²G. Laval and D. Pesme, “Breakdown of quasilinear theory for incoherent 1-d Langmuir waves,” *Phys. Fluids* **26**(1), 52–65 (1983).
- ²³Y. Elskens and D. F. Escande, *Microscopic Dynamics of Plasmas and Chaos* (CRC Press, 2002).
- ²⁴F. Doveil and A. Macor, “Two regimes of self-consistent heating of charged particles,” *Phys. Rev. E* **84**(4), 045401 (2011).
- ²⁵C. Bourdelle, J. Citrin, B. Baiocchi, A. Casati, P. Cottier, X. Garbet, and F. Imbeaux, and JET Contributors, “Core turbulent transport in tokamak plasmas: Bridging theory and experiment with qualikiz,” *Plasma Phys. Controlled Fusion* **58**(1), 014036 (2016).
- ²⁶A. Casati, C. Bourdelle, X. Garbet, F. Imbeaux, J. Candy, F. Claret, G. Dif-Pradalier, G. Falchetto, T. Gerbaud, V. Grandgirard *et al.*, “Validating a quasi-linear transport model versus nonlinear simulations,” *Nucl. Fusion* **49**(8), 085012 (2009).
- ²⁷F. Jenko, T. Dannert, and C. Angioni, “Heat and particle transport in a tokamak: Advances in nonlinear gyrokinetics,” *Plasma Phys. Controlled Fusion* **47**(12B), B195 (2005).
- ²⁸B. Clarisse, “Turbulent transport in tokamak plasmas: Bridging theory and experiment,” Ph.D. thesis, Aix Marseille Université, 2015.
- ²⁹J. C. Adam, G. Laval, and D. Pesme, “Reconsideration of quasilinear theory,” *Phys. Rev. Lett.* **43**(22), 1671 (1979).
- ³⁰T. Cartier-Michaud, P. Ghendrih, Y. Sarazin, G. Dif-Pradalier, T. Drouot, D. Estève, X. Garbet, V. Grandgirard, G. Latu, C. Norscini *et al.*, “Staircase temperature profiles and plasma transport self-organisation in a minimum kinetic model of turbulence based on the trapped ion mode instability,” *J. Phys.: Conf. Ser.* **561**, 012003 (2014).
- ³¹Y. Sarazin, V. Grandgirard, E. Fleurence, X. Garbet, P. Ghendrih, P. Bertrand, and G. Depret, “Kinetic features of interchange turbulence,” *Plasma Phys. Controlled Fusion* **47**(10), 1817 (2005).
- ³²G. Darmet, P. Ghendrih, Y. Sarazin, X. Garbet, and V. Grandgirard, “Intermittency in flux driven kinetic simulations of trapped ion turbulence,” *Commun. Nonlinear Sci. Numer. Simul.* **13**(1), 53–58 (2008).
- ³³T. Drouot, E. Gravier, T. Reveille, M. Sarrat, M. Collard, P. Bertrand, T. Cartier-Michaud, P. Ghendrih, Y. Sarazin, and X. Garbet, “Global gyrokinetic simulations of trapped-electron mode and trapped-ion mode micro-turbulence,” *Phys. Plasmas* **22**(8), 082302 (2015).
- ³⁴T. Drouot, “Étude de la turbulence liée aux particules piégées dans les plasmas de fusion,” Ph.D. thesis, Université de Lorraine, 2015.
- ³⁵P. H. Diamond, S.-I. Itoh, and K. Itoh, *Modern Plasma Physics: Volume 1, Physical Kinetics of Turbulent Plasmas* (Cambridge University Press, 2010).
- ³⁶R. Zinnurovič Sagdeev and A. A. Galeev, *Nonlinear Plasma Theory* (Benjamin, New York, 1969).